Formation, Aggregation, and Deposition Dynamics of NOM-Iron Colloids at Anoxic-Oxic Interfaces

Journal:	*Environmental Science & Technology*
Manuscript ID	es-2017-02356h.R1
Manuscript Type:	Article
Date Submitted by the Author:	n/a
Complete List of Authors:	Liao, Peng; Southern University of Science and Technology of China, School of Environmental Science & Engineering Li, Wenlu; Washington University in St. Louis, Jiang, Yi; Washington University in St. Louis, Department of Energy, Environmental and Chemical Engineering Wu, Jiewei; Washington University in St. Louis, Department of Energy, Environmental and Chemical Engineering Yuan, Songhu; China University of Geosciences, State Key Lab of Biogeology and Environmental Geology Fortner, John; Washington University in St. Louis, School of Engineering & Applied Sciences Giammar, Daniel; Environmental & Chemical Engineering, Department of Civil Energy; Washington University in St. Louis,

Formation, Aggregation, and Deposition Dynamics of NOM-Iron Colloids at Anoxic-Oxic Interfaces

Peng Liao[†,‡,§], Wenlu Li[‡], Yi Jiang[‡,∥], Jiewei Wu[‡], Songhu Yuan[*,†], John D. Fortner[*,‡] and Daniel E. Giammar[‡]

[†]State Key Laboratory of Biogeology and Environmental Geology, China University of Geosciences, 388 Lumo Road, Wuhan, 430074, P. R. China

[‡]Department of Energy, Environmental and Chemical Engineering, Washington University in St. Louis, St. Louis, MO

[§]School of Environmental Science and Engineering, Southern University of Science and Technology, 1088 Xueyuan Road, Shenzhen, 518055, P. R. China

[∥]Department of Civil and Environmental Engineering, The Hong Kong Polytechnic University, Hung Hom, Kowloon, Hong Kong, China

*Corresponding authors:

Songhu Yuan	John D. Fortner
Tel: 86-27-67848629	Tel: 314-935-9293
Fax: 86-27-67883456	Fax: 314-935-7211
yuansonghu622@cug.edu.cn	jfortner@wustl.edu

ABSTRACT The important role of natural organic matter (NOM)−Fe colloids in influencing contaminant transport, and this role can be influenced by the formation, aggregation, and particle deposition dynamics of NOM-Fe colloids. In this work, NOM-Fe colloids at different C/Fe ratios were prepared by mixing different concentrations of humic acid (HA) with 10 mg/L Fe(II) under anoxic conditions. The colloids were characterized by an array of techniques and their aggregation and deposition behaviors were examined under both anoxic and oxic conditions. The colloids are composed of HA-Fe(II) at anoxic conditions, while they are made up of HA-Fe(III) at oxic conditions until the C/Fe molar ratio exceeds 1.6. For C/Fe molar ratios above 1.6, the aggregation and deposition kinetics of HA-Fe(II) colloids under anoxic conditions are slower than those of HA-Fe(III) colloids under oxic conditions. Further, the aggregation of HA-Fe colloids under both anoxic and oxic conditions decreases with increasing C/Fe molar ratio from 1.6 to 23.3. This study highlights the importance of the redox transformation of Fe(II) to Fe(III) and the C/Fe ratio for the formation and stability of NOM-Fe colloids that occur in subsurface environments with anoxic-oxic interfaces.

INTRODUCTION

Biogeochemical cycling of iron (Fe) is active at anoxic and oxic interfaces with dynamic redox conditions that can occur in groundwater, sediments, wetlands, stratified lakes, and marine environments.[1-5] Dissolved Fe(II) is the thermodynamically stable form of Fe at anoxic conditions.[6] The diffusion of dissolved Fe(II) from anoxic zones across interfaces and into more oxic environments can trigger the oxidation of Fe(II) to Fe(III) and the formation of Fe(III) (oxyhydr-)oxides.[7] Considering the low solubility of Fe(III)

in oxic environments at circumneutral pH,[8] the mobility of Fe(III) in subsurface environments can be facilitated by the formation of Fe(III)-rich colloids and Fe(III) complexes with natural ligands.[9,10]

Fe can be intimately associated with natural organic matter (NOM) at anoxic-oxic interfaces.[2,11-13] High concentrations of both Fe(II) and Fe(III) bound to NOM have been detected in anoxic groundwater, wetlands, and pore waters of sediments as well as in oxygen-rich aquifers. [14-16] Molar ratios of organic carbon (C) to Fe between 1 and 30 have been reported in anoxic pore water of sediments, whereby a relatively large fraction of NOM was bound to Fe.[13,14,17] Lalonde et al.[18] recently determined that ca 22% of organic carbon in sediments was directly associated with Fe with an average C/Fe molar ratio of 4.

Evidence from field studies highlights the prevalence of NOM-Fe colloids at anoxic-oxic interfaces with particle size ranging from 1−200 nm.[19-22] Stolpe et al.[23] found that substantial fractions of Fe in rivers were strongly bound to NOM and that these complexes were present as colloids (4−40 nm). Lapworth et al.[24] observed abundant Fe-rich nanoparticles with diameters of 10−30 nm in shallow groundwater that were associated with polydisperse NOM fractions. A recent study provided spectroscopic evidence of Fe(II)-rich colloids in association with NOM in oxygenated water.[16] Due to nanoscale dimensions, large specific surface areas, and high redox reactivity, NOM-Fe colloids can act as geochemical vectors facilitating the transport of a suite of poorly soluble contaminants in the environment.[19,25-27]. For example, NOM-Fe colloids were recently shown to enhance U(IV) transport in a mining-impacted wetland, potentially polluting surface water.[26]

While there is a significant body of knowledge pertaining to the interactions of NOM and Fe,[2,11,13,18,25,27-30] little is known about the properties of NOM-Fe colloids (e.g., composition, aggregation, and deposition) at anoxic-oxic interfaces. Specifically, considerable attention has been paid to the chemical reactions between NOM and Fe, especially in examining the role of NOM on the rate and mechanisms of Fe redox transformation,[28-35] the geochemical reactivity of Fe-NOM complexes,[36-39] and the preservation of Fe and carbon (C).[18,40] Under anoxic conditions, the interaction of NOM with Fe(II) can form NOM-Fe(II) complexes.[38] In comparison, under oxic conditions, NOM can promote or inhibit Fe(II) oxidation and also provide a net protective effect against aggregation and precipitation of Fe(III) (oxyhydr-)oxides, depending on the source, concentration, and redox state of NOM.[28-30,33,35] Further, the C/Fe ratio has a marked effect on the extent of Fe(III) complexation and precipitation kinetics as well as the reactivity of NOM-Fe associations.[13,41-43] While progress has been made in assessing reactions of Fe and NOM, the effect of these reactions on the formation and properties of resulting NOM-Fe colloids remains poorly understood - likely because researchers have used filters of 0.45 or 0.22 μm pore size to separate samples into 'dissolved' and 'particulate' phases.[44] While previous research provides insight into the colloidal behavior (e.g., aggregation and deposition) of carbon- and iron-based nanoparticles,[45-48] the structure and properties of these engineered colloids are essentially different from naturally formed NOM-Fe colloids.

Building on existing knowledge of NOM-Fe reactions, the objectives of this study were to systematically investigate the formation, aggregation, and deposition behaviors of NOM-Fe colloids that form at anoxic-oxic interfaces. The central hypothesis is that a

transition from anoxic to oxic conditions and C/Fe molar ratios substantially affect the composition, aggregation, and deposition of NOM-Fe colloids. To test this, colloids were generated in batch experiments over a range of environmentally relevant C/Fe molar ratios and were fundamentally characterized with subsequent behavior(s) evaluated via aggregation and particle deposition analyses. Findings advance understanding of the stability and mobility of NOM-Fe colloids and the ability to predict the potential fate and transport of contaminants, nutrients, and trace metals associated with NOM-Fe colloids in redox transition zones.

MATERIALS AND METHODS

Materials. All reagents were certified analytical grade and they were used without further purification, and all solutions were prepared using ultrapure water (resistivity >18.2 MΩ·cm, Milli-Q, Millipore). Sigma-Aldrich humic acid (HA), which has been used in several previous studies,[10,49,50] was used as a model NOM compound. A stock solution of HA was prepared by dissolving 2.5 g of HA solid in 500 mL water adjusted to pH 10.5 with NaOH in the dark. The resulting solution was filtered using several 0.45 μm nitrocellulose filters (Millipore). To emulate the reduced state of NOM present at anoxic conditions, a portion of the HA suspension was reacted for 24 h in water equilibrated with a 2−5% atmosphere of H_2 in the presence of a Pd catalyst (0.5% wt on Al_2O_3 spheres, 1 g/L, Sigma-Aldrich).[51] This suspension was subsequently purged with ultrapure N_2 to remove excess H_2 and filtered again with several 0.45 μm filters. The suspension was stored in the dark in an anoxic glovebox (95% N_2 and 5% H_2, Coy Lab Products Inc., MI). To determine the HA concentration, aliquots of suspension were diluted to six different concentrations using ultrapure water and then immediately

transferred to a total organic carbon (TOC) analyzer (Shimadzu TOC-LCPH). Replicate determination of a stock HA gave an average of 1279 ± 11 mg C/L (n = 6). The stock suspension was then used to create suspensions with different working concentrations for later experiments. The concentration of Pd in the filtered HA suspension was 135 ± 4 μg/L (n =2) (The detection limit was 0.2 μg/L) determined by inductively coupled plasma mass spectrometry (ICP-MS) (PerkinElmer ELAN DRC II), indicative of Pd concentration lower than 5 μg/L in the working suspensions, and consequently, the role of Pd on HA reactivity can be neglected in this study. Additional compositional information is provided in the Supporting Information (SI, Table S1).

Colloid Formation. Triplicate experiments were conducted in magnetically-stirred batch reactors (60 mL) at room temperature that were shielded with aluminum foil to avoid any photochemical reactions. An environmentally relevant pH of 7.0 was set for all experiments. The pH was maintained at 7.0 ± 0.1 by 5 mM 4-(2-hydroxyethyl)-1-piperazineethanesulfonic acid (HEPES, ≥ 99.5%, Sigma-Aldrich) buffer and 0.5 M NaOH when necessary. HEPES was selected because it has a minimal influence on interaction between HA and Fe.[52-55] A suite of HA working suspension ranging from 0 to 50 mg C/L was added in the HEPES buffer, and 10 mg/L Fe(II) (added as $FeSO_4$) was then added to these suspensions to create C/Fe molar ratios of 0−23.3. All the reactors contained 5 mM NaCl, which together with the ionic strength contributed by the HEPES, corresponds to a typical ionic strength of freshwater aquifers.[56] Because the presence of background buffer (5 mM HEPES) can significantly affect the precise determination of HA concentration based on TOC analysis, an automated pH-stat titrator (902 Titrando, Metrohm USA Inc.), instead of HEPES, was used to control the suspension pH at 7.0 ±

139 0.2 for an additional series of experiments to measure the HA concentration by TOC
140 measurement. The ionic strength in this system is comparable to that in HEPES system
141 with a relative error less than 20% (data not shown); consequently, the HA concentrations
142 determined can approximately represent the values in HEPES systems.

143 The experimental conditions are summarized in Table S2. The reactions were first
144 performed in the anaerobic chamber. To ensure strictly anoxic conditions throughout the
145 course of experiment periods, all reagents and solutions were sparged by ultrapure N_2 for
146 at least 2 h and then equilibrated with the anaerobic atmosphere in the chamber for at
147 least 12 hours. After the anoxic equilibration stage of the experiment, a portion of the
148 suspension was moved out from the glovebox and aerated to represent a transition to oxic
149 conditions. Oxic experiments were performed by uncapping the reactors and exposing the
150 samples to air for 24 h with magnetic stirring in the dark. The dissolved oxygen (DO)
151 concentration reached 100% of saturation within 1 h as measured by a DO probe
152 (ProODO, YSI Inc.). Control experiments were performed in parallel using 5 mg/L HA
153 alone (no Fe(II) added initially) in the same manner as that used for the scenarios
154 described above. Samples were collected at both the anoxic and oxic equilibrium for
155 analysis and for later aggregation and deposition experiments.

156 The aqueous concentrations of Fe and HA in HA-Fe samples were measured based on
157 the following size fractionation: truly dissolved species (< 10000 Da, roughly equal to <
158 1−3 nm), small colloids (1−3 nm to 20 nm), large colloids (20 − 200 nm), and particulate
159 (> 200 nm). These different fractions were fractionated from samples by 10000 Da
160 cellulose ultrafiltration membranes (EMD, Millipore), 20 nm filters (PES, Whatman), and
161 200 nm filters (PES, Whatman). The Fe(II) concentration in each fraction was determined

by a modified 1,10-phenanthroline method at a wavelength of 510 nm using a UV-vis spectrophotometer. The total Fe concentration after filtration was assayed through reduction of Fe(III) to Fe(II) by hydroxylamine hydrochloride. Total Fe(II) and total Fe concentrations were measured after digesting the unfiltered samples in 0.9 M HCl for 24 h at room temperature in the dark. For the determination of Fe(II), a desired concentration of fluoride was initially added to the sample in an attempt to completely inhibit the redox reactions between Fe and HA during acidification and to prevent the interference of Fe(III).[57] To minimize the interference by HA, most samples (except for ultrafiltered ones) were centrifuged (14,000 *g*) for 2 min to remove HA and the supernatants were assayed immediately.[27] The concentration of Fe(III) was determined as the difference between the total Fe and Fe(II) concentrations. The procedure for anoxic samples was done in the anaerobic chamber to minimize the potential oxidation of Fe(II) to Fe(III). The HA concentration in each fraction was measured by TOC.

The size distributions and the zeta potential of HA-Fe suspensions were measured by dynamic light scattering (DLS) using a Zetasizer Nano (Malvern). Transmission electron microscopy (TEM, Tecnai TM Spirit) examined the morphology of HA-Fe aggregates formed under steady-state oxic conditions. Samples were prepared by depositing a drop of HA-Fe suspension (~ 20 μL) onto a 200 mesh carbon-coated copper grid (Ted Pella, Inc.) followed by immediate evaporation of the remaining water at room temperature under vacuum. Solids from different reactors at the conclusion of both anoxic and oxic experiments were obtained by centrifugation followed by freeze-drying. Freeze-dried solid was used for solid analysis using X-ray photoelectron spectroscopy (XPS) with the aim of determining the surface properties of HA-Fe colloids. XPS spectra were collected

using a PHI Quantera SXM scanning X-ray microprobe with an Al mono source. The analyses were conducted at 26 eV pass energy at a 200 μm X-ray spot size.

Aggregation Kinetics. Aggregation of HA-Fe colloids was examined by monitoring the Z-averaged hydrodynamic diameter using time-resolved DLS. All DLS measurements were made using a photodetector at a scattering angle of 173°. Each autocorrelation function was accumulated every 15 s and DLS samples were left to aggregate for 20−30 min. Because the rapid precipitation of HA-Fe(III) suspensions formed at lower C/Fe molar ratios (< 1.6) under oxic conditions, we devote our consideration of aggregation kinetics to those at higher C/Fe molar ratios (≥ 1.6) where the steady-state suspensions were visually stable (Figure S1). The aggregation kinetics of HA-Fe colloids were evaluated in response to the addition of an electrolyte with a divalent cation (Ca^{2+} and Mg^{2+}) that promoted aggregation. Ca^{2+} and Mg^{2+} were chosen because they are abundant in most natural aquifers at redox interfaces and functioned as representative divalent cations for assessing the aqueous aggregation of engineered nanoparticles.[45-47,58,59] For each measurement, a predetermined volume of suspension in anoxic or oxic conditions at a given C/Fe molar ratios was added into a vial. After that, the vial received a certain amount of electrolyte stock solution and was capped to make the total volume of 1 mL. After 1.5 s of mixing the samples were measured immediately in the DLS chamber. For anoxic experiments, all sample preparation was conducted in the anaerobic chamber and all electrolyte solutions were deoxygenated. Control experiments with HA alone were conducted with the same methods and range of electrolytes concentration.

The attachment efficiency (α) at various electrolyte concentrations was calculated by normalizing the initial aggregation rate constant obtained at a given electrolyte

concentration (k) to the rate constant obtained under diffusion-limited (nonrepulsive, fast) aggregation conditions (k_{fast}) (eq 1).[45,46,58]

$$\alpha = \frac{k}{k_{fast}} = \frac{\frac{1}{N_0}\left(\frac{d}{dt}D_h(t)\right)_{t\to 0}}{\frac{1}{N_{0,fast}}\left(\frac{d}{dt}D_h(t)\right)_{t\to 0,fast}} \qquad (1)$$

where N_0 is the initial particle concentration, and $D_h(t)$ is the hydrodynamic diameter of HA-Fe colloids at time t.

Deposition Kinetics. A quartz crystal microbalance with dissipation (QCM-D, Q-sense AB, Sweden) instrument equipped with four flow-through cells was employed to evaluate the effect of electrolyte (Ca^{2+} and Mg^{2+}) concentration on the deposition of HA-Fe colloids with a C/Fe molar ratio of 4.7 formed at anoxic and oxic conditions onto silica (SiO_2) and poly-L-lysine (PLL) coated silica surfaces. The silica surface was chosen as model surface because it is representative of important interface in natural environments.[45] The deposition experiments were measured by simultaneously monitoring the changes in frequency (Δf) and energy dissipation (ΔD) of several overtones of a SiO_2 coated (5 MHz) QCM-D crystal (QSX-303, Q-sense). Details of the experimental protocols, including sensor cleaning, deposition experiments, and pre-coating of the silica sensor surface with a layer of PLL were reported previously;[45] a description is also provided in the SI Section S1. Briefly, the HEPES/NaCl/pH 7 solution was introduced to the chamber to establish the baseline until the average normalized third overtone frequency shift ceased to drift more than 0.2 Hz in a period of 1 hour. Next, the crystal surfaces were stabilized with a corresponding electrolyte (Ca^{2+} and Mg^{2+}) solution for up to 10 min. The HA-Fe colloid suspension with the same electrolytes was then injected to the sensor for 20 min. Once a stable deposition rate was achieved, the

chamber was flushed with colloid-free electrolyte solution of the same composition for 10 min followed by HEPES/NaCl/pH 7 solution for up to 20 min. The flushing processes were stopped when the average normalized third overtone frequency shift were less than 0.2 Hz over a time period of 10 min.

RESULTS AND DISCUSSION

Colloid Formation. The HA-Fe colloids formed under anoxic and oxic conditions were first characterized by determining the distributions of Fe and C at different size fractions. Under anoxic conditions, Fe remained primarily as Fe(II) regardless of the C/Fe molar ratio (Figure 1a). When the initial C/Fe molar ratio increased from 0 to 23.3, truly dissolved Fe(II) (<1−3 nm) decreased from 98.6% to 13.8% accompanied by the increase in colloidal Fe(II) (Figure 1a). The formation of anoxic HA-Fe(II) colloids was likely due to the coagulation of HA particles. When suspensions are exposed to oxic conditions, all Fe is present as Fe(III) (Figure 1b), due to the oxidation of truly dissolved and colloidal Fe(II) by dissolved oxygen.[30,33] While HA treated by Pd/H_2 was recently shown to be capable of limiting Fe(II) oxidation under oxic conditions for several hours (e.g., 4 h) by acting as a redox buffer and complexant,[60] it does not prevent Fe(II) oxidation over the longer 24-h time of our study. Total Fe analysis of HA-Fe suspension after ultrafiltration (10000 Da) suggests that truly dissolved Fe (< 1−3 nm) is negligible and Fe in suspension is retained by filtration in either the colloidal (1−3 nm to 200 nm) or particulate (> 200 nm) forms (Figure 1b). When the C/Fe molar ratio is less than 1.6, all Fe(III) is in the particulate fraction. As expected from the literature, the dominant iron oxides formed at C/Fe ratio of 0 was lepidocrocite, a well-known product of Fe(II) oxidation by oxygen at neutral conditions.[53,61,62] Solids produced in the presence of HA have been observed to be

254 a mixture of lepidocrocite and ferrihydrite.[52] A substantial fraction of Fe(III) is colloidal
255 once the C/Fe molar ratios ≥ 1.6 (Figure 1b). As discussed by others, hydroxyl and
256 carboxylic groups in HA (surface) can act to stabilize Fe(III), lowering aggregation or
257 precipitation propensities, by forming stable complexes.[9,38,47,63] The extensive
258 aggregation of Fe(III) particles occurring at low C/Fe molar ratios (< 1.6) in contrast to
259 the near complete stabilization of Fe(III) occurring at higher molar ratios (≥ 1.6) suggest
260 that such stabilizing effect(s) depends on C/Fe ratio.[64] For these systems, the observed
261 threshold C/Fe molar ratio is between 1.4 and 1.6 for the complete stabilization of Fe(III)
262 colloids.

263 Regarding the distribution of HA, the concentration in truly dissolved and colloidal
264 fractions at all C/Fe molar ratios under anoxic conditions are statistically comparable to
265 those in control experiments with HA alone, which has approximately 90% of HA
266 occurring in colloidal forms, with less than 10% in the soluble fraction (Figures 1c and
267 S2a). In comparison, under oxic conditions at the lower C/Fe molar ratios (<1.6), all HA
268 is associated with particulate fractions by means of adsorption or co-precipitation with
269 Fe(III) (oxyhydr-)oxides (Figure 1d). This is in contrast to control results in the absence
270 of Fe(II) whereby a higher fraction of HA exists in colloidal forms (Figure S2b). A
271 significant proportion of colloidal HA did not appear until the C/Fe molar ratios reached
272 1.6 (Figure 1d), which is consistent with observations for Fe(III) (Figure 1b). A recent
273 study on the interaction(s) of HA with Fe demonstrated that a portion of HA was not
274 directly bound to Fe at higher C/Fe molar ratios (e.g., ≥ 4.5).[13] This implies that free HA
275 in suspension (i.e. not complexed with HA-Fe colloids) is present in equilibrium with the
276 surfaces of HA-Fe colloids under both anoxic and oxic conditions.

The HA-Fe colloids were further characterized. Z-averaged hydrodynamic diameters of HA-Fe(II) suspensions for anoxic steady-state conditions are in the range of 150−420 nm, irrespective of initial C/Fe molar ratios. Under oxic steady-state conditions, Z-averaged hydrodynamic diameter of HA-Fe(III) suspensions are close to 5000 nm at lower C/Fe ratios, while they are much smaller (130−180 nm) at higher ratios (Figure 2a). Control experiments with HA alone show insignificant change in hydrodynamic diameter for both anoxic and oxic at equilibrium conditions over a range of HA concentrations (Figure S3a). These findings are consistent with the size partitioning results described above (Figure 1). The zeta potentials of HA-Fe suspensions for all steady-state conditions become increasingly negative as C/Fe molar ratios increased (Figure 2b), while no significant change in the zeta potential of HA alone is observed at any concentration tested (Figure S3b). Anoxic conditions lead to an overall more negative charge of HA-Fe suspension than oxic conditions (Figure 2b), which is attributed to the less extent of complexation between carboxyl groups and Fe(II) under anoxic conditions.[2]

TEM images of HA-Fe suspensions formed under oxic conditions support DLS observations, indicating that the change in C/Fe molar ratios affected the size and morphology of HA-Fe colloids (Figure 3). At lower C/Fe molar ratios, most HA was either adsorbed to Fe(III) oxides surfaces (panel a) or co-precipitated with Fe(III) oxides (panel b). Much smaller sheet-like HA-Fe(III) particles, with an average diameter of ~10 nm, were observed at C/Fe molar ratio of 4.7 (panel c). The sheet-like morphology becomes larger (10-60 nm in diameter) as the initial C/Fe molar ratio was increased to 22.3 (panel d). Inspection of micrographs at higher magnification reveals the presence of free HA structure with C/Fe molar ratio of 22.3 (the insert in d), but less so for C/Fe ratio

of 4.7. This suggests that the large HA-Fe(III) particles occurring for higher C/Fe molar ratio(s) are likely due to the presence of larger free HA that was not complexed with Fe(III) in the HA-Fe(III) suspensions. The enrichment of HA on the surface is also supported by the substantially higher surface C/Fe molar ratios detected by XPS than the colloidal and total C/Fe molar ratios (Table S3). Previous research also reported that the surfaces of HA-Fe complexes were relatively enriched with HA.[2,65,66]

Colloid Aggregation. The aggregation behavior of HA-Fe colloids, under both anoxic and oxic conditions, in $CaCl_2$ and $MgCl_2$ solutions clearly shows a reaction-limited regime ($\alpha < 1$, unfavorable) at lower electrolyte concentrations and a diffusion-limited regime ($\alpha = 1$, favorable) for higher electrolyte concentrations (Figure 4), indicating that the aggregation of HA-Fe colloids follows classical Derjaguin-Landau-Verwey-Overbeek (DLVO) theory.[67,68] This also agrees well with previous observations of the aggregation of iron- and carbon-based nanoparticles.[45,46,69-71] When electrolyte concentration was lower than the critical coagulation concentration (CCC), the particle-particle attachment efficiency increased with increasing Ca^{2+} and Mg^{2+} concentration due to the suppression of electrostatic repulsion forces between HA-Fe colloids that accelerated aggregation. At a higher electrolyte concentration (> CCC), the repulsive energy barrier was effectively eliminated between particles and aggregation rates are independent of ionic strength, resulting in a constant α of 1.[46,72,73] In other words, CCC values represent the minimum electrolyte concentration required to completely destabilize colloids as determined by the intersection of extrapolated lines through reaction-limited and diffusion-limited regimes.[45] Higher CCC values generally suggest

that colloids are less susceptible to aggregation and thus have higher degree of stability relative to particles with a lower CCC values under similar conditions.[45,46,72,73]

The aggregation of HA-Fe colloids is highly dependent on the C/Fe molar ratios (Figure 4). Regardless of anoxic and oxic conditions, CCC values for both $CaCl_2$ and $MgCl_2$ solutions increased with increasing C/Fe molar ratio (Figure 4c,f). For example, the CCC of HA-Fe colloids in $CaCl_2$ solutions under oxic conditions noticeably increases from 2.5 to 4.6 mM and then further increases to 5.1 mM as the C/Fe molar ratio increased from 1.6 to 4.7 and to 23.3, respectively (Figure 4c). This indicates that HA-Fe colloids formed at higher C/Fe molar ratios are less vulnerable to aggregation (i.e. relatively more stable). A regression analysis on CCC values versus the percentage of colloidal Fe (ratio of Fe in the colloidal fraction to total Fe in HA-Fe suspensions) are linearly correlated ($R^2 > 0.98$) with higher colloidal Fe concentration leading to higher CCC values (Figure S4). As colloidal Fe concentration was modulated by the C/Fe molar ratio or HA concentration (i.e. constant 10 mg/L Fe concentration in this study), the aggregation of HA-Fe colloids depends on the HA concentration. Previous studies have observed that adsorbed HA can stabilize iron-bearing nanoparticles against aggregation and transformation.[43,47,64,74-76] These results imply that lower aggregation propensity of HA-Fe colloids formed at higher C/Fe molar ratios may also be due to free HA adsorbed on the surfaces of colloids, enhancing electrostatic and/or steric repulsion interactions.

Additional insight into these colloidal-based phenomena is possible through zeta potential measurements (Figure 5). The zeta potential for both $CaCl_2$ and $MgCl_2$ solutions become more negative with increasing C/Fe molar ratios (Figure 5), indicating that the electrostatic repulsion between HA-Fe particles increases with increasing C/Fe molar

345 ratios.[47,67] A linear correlation between the CCC values and zeta potential values is
346 observed ($R^2 > 0.7$, Figure S5); the higher absolute zeta potential values led to lower
347 aggregation tendencies. The zeta potential of HA-Fe colloids did not vary significantly
348 once the C/Fe molar ratios were above 4.7 (Figure 5). This implies that electrostatic
349 repulsion is not the only reason for suspension stabilization as steric hindrance may also
350 play an appreciable role, as observed by others.[46,47,71,72,77-79] Further, zeta potential
351 decreased when Ca^{2+}/Mg^{2+} ion concentration(s) increased due to charge screening effects
352 and the extent of such decrease in the presence of Ca^{2+} was greater compared to that of
353 Mg^{2+} (Figure S6a,b). This can be attributed to the stronger bridging effects of Ca^{2+}
354 compared to Mg^{2+},[47] resulting in lower aggregation resistance, as reflected by the lower
355 CCC values (Figure 4c,f). Comparison of the zeta potential in the presence of
356 Ca^{2+}/Mg^{2+}/Na^{+} (Figure 5) and Na^{+} (Figure 2b) shows that a relatively low concentration
357 of Ca^{2+}/Mg^{2+} can significantly decrease the absolute value of the zeta potential of HA-Fe
358 colloids (e.g., from − ~ 50 mV in 5 mM NaCl background solution to – 15~25 mV in 1
359 mM Ca^{2+}/Mg^{2+} and 5 mM Na^{+} solutions), which is attributed to divalent cations more
360 effectively neutralizing surface charge than monovalent cations.[45-47]

361 For a given C/Fe molar ratio, HA-Fe colloids formed under anoxic conditions are
362 more stable against aggregation than those formed under oxic conditions, especially for
363 lower C/Fe molar ratios (Figure 4). The CCC values of Ca^{2+} and Mg^{2+} for anoxic HA-
364 Fe(II) colloids were always higher than those for oxic HA-Fe(III) colloids and such
365 difference was more pronounced when the C/Fe molar ratio was 1.6 (Figure 4c,f).
366 Enhanced stability of anoxic HA-Fe(II) colloids might be related to the presence of free
367 COO- group in HA (i.e. did not form bonds with Fe(II)) in anoxic conditions due to the

lower propensity of Fe(II) to associate with HA.[2,80] This gives rise to considerably more negative zeta potential of anoxic HA-Fe colloids in both Ca^{2+} and Mg^{2+} solutions than for oxic HA-Fe colloids (Figures 5 and S6c,d). Higher stability of anoxic HA-Fe(II) colloids may also be, in part, due to their lower density relative to oxic HA-Fe(III) colloids, particularly at low C/Fe molar ratios. It is worth mentioning that a large fraction of truly dissolved Fe(II) existed in anoxic HA-Fe(II) colloids, which may increase the ionic strength of colloids and thus potentially decrease their stability. By removing truly dissolved Fe(II) in HA-Fe(II) colloids (C/Fe molar ratio of 1.6) using ultrafiltration in anoxic conditions, we compared the aggregation of anoxic HA-Fe(II) colloids with and without truly dissolved Fe(II). The CCC values for both cases are comparable (Figure S7), indicating minimal effect of truly dissolved Fe(II) with regard to stability.

Colloid Deposition. Experiments with HA alone showed no deposition onto silica sensor surfaces in the absence of Ca^{2+}/Mg^{2+} (Figure S8) due to repulsive electrostatic interactions between HA and silica. The deposition of HA onto positively charged PLL coated surfaces without Ca^{2+}/Mg^{2+} increased linearly with HA concentration ($R^2 = 0.977$, Figure S9) suggesting that normalized deposition of HA-Fe colloids is independent of HA concentration and can be monitored from the rate of frequency shift in QCM-D, as predicted by the Sauerbrey relationship.[81]

Deposition attachment efficiency (α_D) of HA-Fe colloids formed under oxic conditions is higher than that for colloids formed under anoxic conditions for both Ca^{2+} and Mg^{2+} solutions (Figure 6a,b). This difference in deposition efficiency is similar to the trend for aggregation behaviors (Figure 4); the higher the aggregation of HA-Fe colloids, the higher the extent of HA-Fe colloids deposition onto silica surfaces. Enhanced

391 deposition for oxic conditions can be explained by the lower aggregation of the originally
392 formed colloids at anoxic conditions than at oxic conditions (Figure 4). The α_D of HA-Fe
393 colloids in the presence of Ca^{2+} is slightly higher (1−1.4 times) than in the presence of
394 Mg^{2+} for the same concentrations, due to the higher complexation and related bridging
395 effects of Ca^{2+} ions with COO- groups of HA-Fe colloids.[47,82,83]

396 The deposited layer stiffness was also assessed in terms of the slope of D to *f*
397 ($|\Delta D_{(3)}/\Delta f_{(3)}|$), which is used to estimate the induced energy dissipation per coupled mass
398 change.[45,84-86] High $|\Delta D_{(3)}/\Delta f_{(3)}|$ values indicate relatively loose deposits, while low
399 $|\Delta D_{(3)}/\Delta f_{(3)}|$ values indicate relatively rigid deposition layers.[45,82,87] Regardless of
400 favorable or unfavorable deposition conditions, $|\Delta D_{(3)}/\Delta f_{(3)}|$ values obtained in oxic
401 conditions are higher (2.6−4.2 times) than the values obtained in anoxic conditions
402 (Figure 6c,d), suggesting that the deposited colloids from oxic conditions on both silica
403 and PLL-coated surfaces are more dissipative and, thus looser, than the deposits of
404 colloids formed under anoxic conditions. Under non-repulsive conditions, the $|\Delta D_{(3)}/\Delta f_{(3)}|$
405 values for PLL coated surfaces are lower than the values on silica surfaces (Figure 6c,d),
406 indicating that the deposition layers of HA-Fe colloids on favorable surfaces are more
407 rigid (compact structure) than on unfavorable surfaces, which is likely due, in part, to the
408 fact that HA-Fe colloids deposition on PLL-coated surfaces was mainly at the primary
409 energy minimum while deposition of HA-Fe colloids on silica surfaces was controlled by
410 the secondary energy minima.[82,88] For both surfaces, an increase in Ca^{2+}/Mg^{2+}
411 concentrations resulted in higher $|\Delta D_{(3)}/\Delta f_{(3)}|$ values (Figure 6c,d), indicating that the
412 deposition layer becomes more loosely attached to silica and PLL-coated surfaces with
413 increasing ionic strength as a result of the formation/deposition of larger

aggregates.[82,86,87] $|\Delta D_{(3)}/\Delta f_{(3)}|$ values of HA-Fe colloids on both surfaces in the presence of Ca^{2+} are notably higher than in the presence of Mg^{2+} (Figure 6c,d), which suggests that the deposited HA-Fe colloids layers in Ca^{2+} conditions are softer and more dissipative, which is consistent with other studies.[45,82]

Environmental Implications. This study fundamentally expands our knowledge of HA interactions with Fe by providing new information on the formation and stability of NOM-Fe colloids, which are formed at anoxic-oxic interfaces. Such insight is valuable for deeper understanding of critical biogeochemical cycling aspects of C and Fe and the transport of colloid-associated contaminants, nutrients, and trace metals at redox sensitive interfaces, which are ubiquitous in the environment. Under conditions described, the stability of colloidal Fe depends on the C/Fe molar ratios. Organic-rich systems are thus likely to enhance the mobility of colloidal Fe. Findings from this study may also be extended to biotic systems in which HA-Fe(III) colloids can be formed during the bio-oxidation of aqueous Fe(II) in the presence of HA.[89-91] Colloids with enhanced stability may also have an impact on the fate and transport of contaminants, especially in the context of higher C/Fe molar ratios – resulting in more stable colloids, which are thus more mobile. As HA-Fe(II) colloids formed under anoxic conditions are reducing,[38,60] it is also reasonable to anticipate that they are capable of reducing redox active contaminants (e.g., Cr(VI) and U(VI)). While reduced contaminants (e.g., Cr(III) and U(IV)) are generally considered to be less mobile under oxic conditions, their mobility, in association with stable HA-Fe colloids, would be relatively enhanced. We certainly realize that natural environments are more complicated than systems presented, based on

437 the presence of different types of NOM and periodic oscillation of redox conditions, and
438 further research is required to extend the framework developed here to assess the redox
439 properties, (extended) structures, and stability of NOM-Fe colloids in actual subsurface
440 environments.
441

442 ## Supporting Information

443 Additional information regarding QCM-D deposition experiment, selected
444 physicochemical properties of HA and HA-Fe colloids, photographs of HA-Fe
445 suspensions, concentration partitioning, hydrodynamic diameter, and zeta potential of HA
446 under anoxic and oxic conditions, and correlations between CCC and properties of HA-
447 Fe colloids (PDF)
448

449 **Acknowledgements.** This study was supported by the U.S. National Science
450 Foundation (CBET 1335613), the Natural Science Foundation of China (No. 41703128,
451 41521001), the Ministry of Education for New Century Excellent Talents Support Plans
452 (NCET-13-1014), and the Southern University of Science and Technology (G01296001).
453 We thank the staff of the Nano Research Facility (NRF) at Washington University for
454 their assistance with TEM and DLS; the NRF was a member of the National
455 Nanotechnology Infrastructure Network (NNIN), which was funded by the National
456 Science Foundation under Grant No. ECS-0335765. XPS analysis was performed in the
457 Institute of Materials Science and Engineering (IMSE), Washington University in St.
458 Louis, with support from National Science Foundation under Grant CBET-1337374. We
459 also thank Chao Pan for helpful discussions.

REFERENCES

(1) Liang, L. Y.; Mccarthy, J. F.; Jolley, L. W.; Mcnabb, J. A.; Mehlhorn, T. L. Iron dynamics: Transformation of Fe(II)/Fe(III) during injection of natural organic matter in a sandy aquifer. *Geochim. Cosmochim. Acta* **1993**, *57*, 1987−1999.

(2) Riedel, T.; Zak, D.; Biester, H.; Dittmar, T. Iron traps terrestrially derived dissolved organic matter at redox interfaces. *Proc. Natl. Acad. Sci. U. S. A.* **2013**, *110*, 10101−10105.

(3) Buffle, J.; Vitre, R. R. D.; Leppard, G. G. Physico-chemical characteristics of a colloidal iron phosphate species formed at the oxic-anoxic interface of a eutrophic lake. *Geochim. Cosmochim. Acta* **1989**, 53, 399−408.

(4) Pakhomova, S. V.; Hall, P. J.; Kononets, M. Y.; Rozanov, A. G.; Tengberg, A. T.; Vershinin, A. V. Fluxes of iron and manganese across the sediment–water interface under various redox conditions. *Mar. Chem.* **2007**, *107*, 319−331.

(5) Hawkings, J .R.; Wadham, J .L.; Tranter, M.; Raiswell, R.; Benning, L. G.; Statham, P. J.; Tedstone, A.; Nienow, P.; Lee, K.; Telling, J. Ice sheets as a significant source of highly reactive nanoparticulate iron to the oceans. *Nat. Commun.* **2014**, *5*, 1−8.

(6) Lohan, M. C.; Bruland, K .W. Elevated Fe(II) and dissolved Fe in hypoxic shelf waters off Oregon and Washington: An enhanced source of iron to coastal upwelling regimes. *Environ. Sci. Technol.* 2008, *42*, 6462–6468.

(7) King, D. W. Role of carbonate speciation on the oxidation rate of Fe(II) in aquatic systems. *Environ. Sci. Technol.* **1998**, *32*, 2997−3003.

(8) Fox, L. E. Solubility of colloidal ferric hydroxide. *Nature* **1988**, *333*, 442-444.

(9) Gledhill, M.; Buck, K. N. The organic complexation of iron in the marine environment: A review. *Front. Microbiol.* **2012**, *3*, 1−17.

(10) Rue, E. L.; Bruland, K. W. Complexation of iron(III) by natural organic ligands in the central north pacific as determined by a new competitive ligand equilibration/adsorptive cathodic stripping voltammetric method. *Mar. Chem.* **1995**, *50*, 117–138.

(11) Schwertmann, U. Inhibitory effect of soil organic matter on crystallization of amorphous ferric hydroxide. *Nature* **1966**, *212*, 645−646.

(12) Wagai, R.; Mayer, L. M. Sorptive stabilization of organic matter in soils by hydrous iron oxides. *Geochim. Cosmochim. Acta* **2007**, *71*, 25–35.

(13) Chen, C.; Dynes, J.; Wang, J.; Sparks, D. L. Properties of Fe-organic matter associations via coprecipitation versus adsorption. *Environ. Sci. Technol.* **2014**, *48*, 13751−13759.

(14) Chin, Y.P.; Traina, S. J.; Swank, C. R.; Backhus, D. Abundance and properties of dissolved organic matter in pore waters of a freshwater wetland. *Limnol. Oceanogr.* **1998**, *43*, 1287–1296.

(15) O'Loughlin, E. J.; Chin, Y. P. Quantification and characterization of dissolved organic carbon and iron in sedimentary porewater from Green Bay, WI, USA. *Biogeochemistry* **2004**, *71*, 371–386.

(16) von der Heyden, B. P.; Hauser, E. J.; Mishra, B.; Martinez, G .A.; Bowie, A. R.; Tyliszczak, T.; Mtshali, T. N.; Roychoudhury, A. N.; MynenI, S. C. B. Ubiquitous presence of Fe(II) in aquatic colloids and its association with organic carbon. *Environ. Sci. Technol. Lett.* 2014, *1*, 387–392.

(17) Katoh, M.; Murase, J.; Hayashi, M.; Matsuya, K.; Kimura, M. Nutrient leaching from the plow layer by water percolation and accumulation in the subsoil in an irrigated paddy field. *Soil Sci. Plant Nutr.* **2004**, *50*, 721−729.

(18) Lalonde, K.; Mucci, A.; Quellet, A.; Gélinas, Y. Preservation of organic matter in sediments promoted by iron. *Nature* **2012**, *483*, 198−200.

(19) Pokrovsky, O. S.; Schott, J. Iron colloids/organic matter associated transport of major and trace elements in small boreal rivers and their estuaries (NW Russia). *Chem. Geol.* **2002**, *190*, 141–179.

(20) Boye, M.; Nishioka, J.; Croot, P.; Laan, P.; Timmermans, K. R.; Strass, V. H.; Takeda, S.; de Baar, H. J. W. Significant portion of dissolved organic Fe complexes in fact is Fe colloids. *Mar. Chem.* **2010**, *122*, 20−27.
(21) Garnier, J. M.; Hurel, C.; Garnier, J.; Lenoble, V.; Garnier, C.; Ahmed, K. M.; Rose, J. Strong chemical evidence for high Fe(II)-colloids and low As-bearing colloids (200 nm-10 kDa) contents in groundwater and flooded paddy fields in Bangladesh: A size fractionation approach. *Appl. Geochem.* **2011**, *26*, 1665−1672.
(22) Regelink, I. C.; Voegelin, A.; Weng, L.; Koopmans, G. F.; Comans, R. N. J. Characterization of colloidal Fe from soils using field-flow fractionation and Fe K-edge X-ray absorption spectroscopy. *Environ. Sci. Technol.* **2014**, *48*, 4307−4316.
(23) Stolpe, B. S.; Guo, L.; Shiller, A. M. Binding and transport of rare earth elements by organic and iron-rich nanocolloids in Alaskan rivers, as revealed by field-flow fractionation and ICP-MS. *Geochim. Cosmochim. Acta* **2013**, *106*, 446–462.
(24) Lapworth, D. J.; Stolpe, B.; Williams, P. J.; Gooddy, D. C.; Lead, J. R. Characterization of suboxic groundwater colloids using a multimethod approach. *Environ. Sci. Technol.* **2013**, *47*, 2554−2561.
(25) Pokrovsky, O. S.; Manasypov, R. M.; Loiko, S. V.; Shirokova, L. S. Organic and organo-mineral colloids in discontinuous permafrost zone. *Geochim. Cosmochim. Acta* **2016**, *188*, 1–20.
(26) Wang, Y. H.; Frutschi, M.; Suvorova, E.; Phrommavanh, V.; Descostes, M.; Osman, A. A. A.; Geipel, G.; Bernier-Latmani, R. Mobile uranium(IV)-bearing colloids in a mining-impacted wetland. *Nat. Commun.* **2013**, *4*, 1−9.
(27) Sharma, P.; Ofner, J.; Kappler, A. Formation of binary and ternary colloids and dissolved complexes of organic matter, Fe and As. *Environ. Sci. Technol.* **2010**, *44*, 4479–4485.
(28) Jackson, A.; Gaffney, J. W.; Boult, S. Subsurface interactions of Fe(II) with humic acid or landfill leachate do not control subsequent iron(III) (hydr)oxide production at the surface. *Environ. Sci. Technol.* **2012**, *46*, 7543−7550.
(29) Gaffney, J. W.; White, K. N.; Boult, S. Oxidation state and size of Fe controlled by organic matter in natural waters. *Environ. Sci. Technol.* **2008**, *42*, 3575−3581.
(30) Pullin, M. J.; Cabaniss, S. E. The effects of pH, ionic strength, and iron–fulvic acid interactions on the kinetics of non-photochemical iron transformations. I. Iron(II) oxidation and iron(III) colloid formation. *Geochim. Cosmochim. Acta* **2003**, *67*, 4067−4077.
(31) Garg, S.; Jiang, C.; Miller, C. J.; Rose, A. L.; Waite T. D. Iron redox transformations in continuously photolyzed acidic solutions containing natural organic matter: Kinetic and mechanistic insights. *Environ. Sci. Technol.* **2013**, *47*, 9190−9197.
(32) Garg, S.; Jiang, C.; Waite T. D. Mechanistic insights into iron redox transformations in the presence of natural organic matter: Impact of pH and light. *Geochim. Cosmochim. Acta* **2015**, *165*, 14–34.
(33) Liang, L.; McNabb, J. A.; Paulk, J. M.; Gu, B.; McCarthy, J. F. Kinetics of Fe(II) oxygenation at low partial pressure of oxygen in the presence of natural organic matter. *Environ. Sci. Technol.* **1993**, *27*, 1864−1870.
(34) Rose, A. L.; Waite, T. D. Kinetic model for Fe(II) oxidation in seawater in the absence and presence of natural organic matter. *Environ. Sci. Technol.* **2002**, *36*, 433−444.
(35) Rose, A. L.; Waite, T. D. Effect of dissolved natural organic matter on the kinetics of ferrous iron oxygenation in seawater. *Environ. Sci. Technol.* **2003**, *37*, 4877−4886.
(36) Hakala, J. A.; Fimmen, R. L.; Chin, Y. P.; Agrawal, S. G.; Ward, C. P. Assessment of the geochemical reactivity of Fe-DOM complexes in wetland sediment pore waters using a nitroaromatic probe compound. *Geochim. Cosmochim. Acta* **2009**, *73*, 1382−1393.
(37) Beckler, J. S.; Jones, M. E.; Taillefert, M. The origin, composition, and reactivity of dissolved iron(III) complexes in coastal organic- and iron-rich sediments. *Geochim. Cosmochim. Acta* **2015**, *152*, 72–88.

(38) Catrouillet, C.; Devranche, M.; Dia, A.; Coz, M. B. L.; Marsac, R.; Pourret, O.; Gruau, G. Geochemical modeling of Fe(II) binding to humic and fulvic acids. *Chem. Geol.* **2014**, *372*, 109−118.
(39) Mikutta, R.; Lorenz, D.; Guggenberger, G.; Haumaier, L.; Freund, A. Properties and reactivity of Fe-organic matter associations formed by coprecipitation versus adsorption: Clues from arsenate batch adsorption. *Geochim. Cosmochim. Acta* **2014**, *144*, 258−276.
(40) Toner, B. M.; Fakra, S. C.; Manganini, S. J.; Santelli, C. M.; Marcus, M. A.; Moffett, J. W.; Rouxel, O.; German, C. R.; Edwards, K. Preservation of iron(II) by carbon-rich matrices in a hydrothermal plume. *Nature Geosci.* **2009**, *2*, 197−201.
(41) Aiken, G. R.; Hsu-Kim, H.; Ryan, J. N. Influence of dissolved organic matter on the environmental fate of metals, nanoparticles, and colloids. *Environ. Sci. Technol.* **2011**, *45*, 3196−3201.
(42) Amstaetter, K.; Borch, T.; Kappler, A. Influence of humic acid imposed changes of ferrihydrite aggregation on microbial Fe(III) reduction. *Geochim. Cosmochim. Acta* **2012**, *85*, 326−341.
(43) Shimizu, M.; Zhou, J.; Schröder, C.; Obst, M.; Kappler, A.; Borch, T. Dissimilatory reduction and transformation of ferrihydrite-humic acid coprecipitates. *Environ. Sci. Technol.* **2013**, *47*, 13375−13384.
(44) Wu, J. F.; Boyle, E.; Sunda, W.; Wen, L. S. Soluble and colloidal iron in the oligotrophic North Atlantic and North Pacific. *Science* **2001**, *293*, 847–849.
(45) Li, W.; Liu, D.; Wu, J.; Kim, C.; Fortner, J. D. Aqueous aggregation and surface deposition processes of engineered superparamagnetic iron oxide nanoparticles for environmental applications. *Environ. Sci. Technol.* **2014**, *48*, 11892−11900.
(46) Jiang, Y.; Raliya, R.; Fortner, J. D.; Biswas, P. Graphene oxides in water: Correlating morphology and surface chemistry with aggregation behavior. *Environ. Sci. Technol.* **2016**, *50*, 6964−6973.
(47) Philippe, A.; Schaumann, G. E. Interactions of dissolved organic matter with natural and engineered inorganic colloids: A review. *Environ. Sci. Technol.* **2014**, *48*, 8946−8962.
(48) Sharma, V. K.; Filip, J.; Zboril, R.; Varma, R. S. Natural inorganic nanoparticles−formation, fate, and toxicity in the environment. *Chem. Soc. Rev.* **2015**, *44*, 8410−8423.
(49) Liu, G. L.; Fernandez, A.; Cai, Y. Complexation of arsenite with humic acid in the presence of ferric iron. *Environ. Sci. Technol.* **2011**, *45*, 3210−3216.
(50) Yu, Z. G.; Peiffer, S.; Göttlicher, J.; Knorr, K. H. Electron transfer budgets and kinetics of abiotic oxidation and incorporation of aqueous sulfide by dissolved organic matter. *Environ. Sci. Technol.* **2015**, *49*, 5441−5449.
(51) Zheng, W.; Liang, L.Y.; Gu, B. H. Mercury reduction and oxidation by reduced natural organic matter in anoxic environments. *Environ. Sci. Technol.* **2012**, *46*, 292–299.
(52) Pan, C., Troyer, L. D., Liao, P., Catalano, J. G., Li, W. L., Giammar, D. E.. Effect of humic acid on the removal of chromium(VI) and the production of solids in iron electrocoagulation. *Environ. Sci. Technol.* **2017**, *51*, 6308–6318.
(53) Pan, C.; Troyer, L. D.; Catalano, J. G.; Giammar, D. E. Dynamics of chromium(VI) removal from drinking water by iron electrocoagulation. *Environ. Sci. Technol.* **2016**, *50*, 13502−13510.
(54) Wang, Z. Y.; von dem Bussche, A.; Qiu, Y.; Valentin, T. M.; Gion, K.; Kane, A. B.; Hurt, R. H. Chemical dissolution pathways of MoS_2 nanosheets in biological and environmental media. *Environ. Sci. Technol.* **2016**, *50*, 7208−7217.
(55) Liu, J.; Pearce, C. I.; Shi, L.; Wang, Z. M.; Shi, Z.; Arenholz, E.; Rosso, K. M. Particle size effect and the mechanism of hematite reduction by the outer membrane cytochrome OmcA of *Shewanella oneidensis* MR-1. *Geochim. Cosmochim. Acta* **2016**, *193*, 160–175.
(56) Harter, T.; Wagner, S.; Atwill, E. R. Colloid transport and filtration of *Cryptosporidium parvum* in sandy soils and aquifer sediments. *Environ. Sci. Technol.* **2000**, *34*, 62−70.

(57) Tamura, H.; Goto, K.; Yotsuyanagi, T.; Nagayama, M. Spectrophotometric determination of iron (II) with 1, 10-phenanthroline in the presence of large amounts of iron (III). *Talanta* **1974**, *21*, 314−318.
(58) Gutierrez, L.; Nguyen, T. H. Interactions between rotavirus and Suwannee river organic matter: Aggregation, deposition, and adhesion force measurement. *Environ. Sci. Technol.* **2012**, *46*, 8705−8713.
(59) Cai, W. J.; Wang, Y. C.; Krest, J.; Moore, W. S. The geochemistry of dissolved inorganic carbon in a surficial groundwater aquifer in North Inlet, South Carolina, and the carbon fluxes to the coastal ocean. *Geochim. Cosmochim. Acta* **2002**, *4*, 631–639.
(60) Daugherty, E. E.; Gilbert, B.; Nico, P. S.; Borch, T. Complexation and redox buffering of iron(II) by dissolved organic matter. *Environ. Sci. Technol.* **2017**, DOI: 10.1021/acs.est.7b03152.
(61) Dubrawski, K. L.; van Genuchten, C. M.; Delaire, C.; Amrose, S. E.; Gadgil, A. J.; Mohseni, M. Production and transformation of mixed valent nanoparticles generated by Fe(0) electrocoagulation. *Environ. Sci. Technol.* **2015**, *49*, 2171−2179.
(62) Voegelin, A.; Senn, A. C.; Kaegi, R.; Hug, S. J.; Mangold, S. Dynamic Fe-precipitate formation induced by Fe(II) oxidation in aerated phosphate-containing water. *Geochim. Cosmochim. Acta* **2013**, *117*, 216−231.
(63) Karlsson, T.; Persson, P. Coordination chemistry and hydrolysis of Fe(III) in a peat humic acid studied by X-ray absorption spectroscopy. *Geochim. Cosmochim. Acta* **2010**, *74*, 30−40.
(64) Liao, P.; Li, W. L.; Jiang, Y.; Fortner, J. D.; Yuan, S. H. Effect of reduced humic acid on the transport of ferrihydrite nanoparticles under anoxic conditions. *Water Res.* **2017**, *109*, 347–357.
(65) Oleinikova, O. V.; Shirokova, L. S.; Gérard, E.; Drozdova, O. Y.; Lapitskiy, S. A.; Bychkov, A.Y.; Pokrovsky, O. S. Transformation of organo-ferric peat colloids by a heterotrophic bacterium. *Geochim. Cosmochim. Acta* **2017**, *205*, 313–330.
(66) Adhikari, D.; Zhao, Q.; Das, K.; Mejia, J.; Huang, R.; Wang, X.; Poulson, S. P.; Tang, Y. Z.; Roden, E. E.; Yang, Y. Dynamics of ferrihydrite-bound organic carbon during microbial Fe reduction. *Geochim. Cosmochim. Acta* **2017**, *212*, 221–233.
(67) Petosa, A. R.; Jaisi, D. P.; Quevedo, I. R.; Elimelech, M.; Tufenkji, N. Aggregation and deposition of engineered nanomaterials in aquatic environments: Role of physicochemical interactions. *Environ. Sci. Technol.* **2010**, *44*, 6532−6549.
(68) Lin, M. Y.; Lindsay, H. M.; Weitz, D. A.; Ball, R. C.; Klein, R.; Meakin, P. Universality in colloid aggregation. *Nature* **1989**, 339, 360−362.
(69) Wang, L. F.; Wang, L. L.; Ye, X. D.; Li, W. W.; Ren, X. M.; Sheng, G. P.; Yu, H. Q.; Wang, X. K. Coagulation kinetics of humic aggregates in mono- and di-valent electrolyte solutions. *Environ. Sci. Technol.* **2013**, *47*, 5042−5049.
(70) Chen, K. L.; Mylon, S.; Elimelech, M. Aggregation kinetics of alginate-coated hematite nanoparticles in monovalent and divalent electrolytes. *Environ. Sci. Technol.* **2006**, *40*, 1516−1523.
(71) Chen, K. L.; Elimelech, M. Aggregation and deposition kinetics of fullerene (C60) nanoparticles. *Langmuir* **2006**, *22*, 10994−11001.
(72) Sheng, A.; Liu, F.; Shi, L.; Liu, J. Aggregation kinetics of hematite particles in the presence of outer membrane cytochrome OmcA of *Shewanella oneidenesis* MR‑1. *Environ. Sci. Technol.* **2016**, *50*, 11016−11024.
(73) Li, W. L.; Lee, S. S.; Mittelman, A. M.; Liu, D.; Wu, J. W.; Hinton, C. H.; Abriola, L. M.; Pennell, K. D.; Fortner, J. D. Aqueous aggregation behavior of engineered superparamagnetic iron oxide nanoparticles: Effects of oxidative surface aging. *Environ. Sci. Technol.* **2016**, *50*, 12789−12798.
(74) Kretzschmar, R.; Sticher, H. Transport of humic-coated iron oxide colloids in a sandy soil: influence of Ca^{2+} and trace metals. *Environ. Sci. Technol.* **1997**, *31*, 3497−3504.
(75) Illés, E.; Tombácz, E. The effect of humic acid adsorption on pH-dependent surface charging and aggregation of magnetite nanoparticles. *J. Colloid Interface Sci.* **2006**, *295*, 115–123.

(176) Jones, A. M.; Collins, R. N.; Rose, J.; Waite, T. D. The effect of silica and natural organic matter on the Fe(II)-catalysed transformation and reactivity of Fe(III) minerals. *Geochim. Cosmochim. Acta* **2009**, *73*, 4409–4422.
(177) Huangfu, X. L.; Jiang, J.; Ma, J.; Liu, Y. Z.; Yang, J. Aggregation kinetics of manganese dioxide colloids in aqueous solution: Influence of humic substances and biomacromolecules. *Environ. Sci. Technol.* **2013**, *47*, 10285−10292.
(178) Yin, Y. G.; Shen, M. H.; Tan, Z. Q.; Yu, S. J.; Liu, J. F.; Jiang, G. B. Particle coating-dependent interaction of molecular weight fractionated natural organic matter: Impacts on the aggregation of silver nanoparticles. *Environ. Sci. Technol.* **2015**, *49*, 6581−6589.
(179) Jiang, Y.; Raliya, R.; Liao, P.; Biswas, P.; Fortner, J. D. Graphene oxides in water: assessing stability as a function of material and natural organic matter propterties. *Environ. Sci. Nano* **2017**, *4*, 1484–1493.
(180) Nierop, K. G. J; Jansen, B,; Verstraten, J. M. Dissolved organic matter, aluminium and iron interactions: Precipitation induced by metal/carbon ratio, pH and competition. *Sci. Total Environ.* **2002**, *300*, 201–211.
(181) Sauerbrey, G. Use of quartz vibrator for weighing thin layers and as a micro-balance. *Z. Phys.* **1959**, *155*, 206−222.
(182) Chowdhury, I.; Duch, M. C.; Mansukhani, N. D.; Hersam, M. C.; Bouchard, D. Deposition and release of graphene oxide nanomaterials using a quartz crystal microbalance. *Environ. Sci. Technol.* **2013**, *48*, 961−969.
(183) Yi, P.; Chen, K. L. Influence of surface oxidation on the aggregation and deposition kinetics of multiwalled carbon nanotubes in monovalent and divalent electrolytes. *Langmuir* **2011**, *27*, 3588−3599.
(184) Olsson, A. L. J.; Quevedo, I. R.; He, D.; Basnet, M.; Tufenkji, N. Using the quartz crystal microbalance with dissipation monitoring to evaluate the size of nanoparticles deposited on surfaces. *ACS Nano* **2013**, *7*, 7833−7843.
(185) Fatisson, J.; Domingos, R. F.; Wilkinson, K. J.; Tufenkji, N. Deposition of TiO_2 nanoparticles onto silica measured using a quartz crystal microbalance with dissipation monitoring. *Langmuir* **2009**, *25*, 6062−6069.
(186) Quevedo, I. R.; Olsson, A. L. J.; Tufenkji, N. Deposition kinetics of quantum dots and polystyrene latex nanoparticles onto alumina: Role of water chemistry and particle coating. *Environ. Sci. Technol.* **2013**, *47*, 2212−2220.
(187) Chowdhury, I.; Duch, M. C.; Mansukhani, N. D.; Hersam, M. C.; Bouchard, D. Interactions of graphene oxide nanomaterials with natural organic matter and metal oxide surfaces. *Environ. Sci. Technol.* **2014**, *48*, 9382−9390.
(188) Yi, P.; Chen, K. L. Influence of solution chemistry on the release of multiwalled carbon nanotubes from silica surfaces. *Environ. Sci. Technol.* **2013**, *47*, 12211−12218.
(189) Taillefert, M.; Rozan, T. F.; Glazer, B. T.; Herszage, J.; Trouwborst, R. E.; Luther, G. W. Seasonal variations of soluble organic-Fe(III) in sediment porewaters as revealed by voltammetric microelectrodes. 2002. In: *Environmental Electrochemistry: Analyses of Trace Element Biogeochemistry* (Taillefert, M.; Rozan, T., Eds.). American Chemical Society: Washington, D. C., 247–264.
(190) Melton, E. M.; Swanner, E. D.; Behrens, S.; Schmidt, C.; Kappler, A. The interplay of microbially mediated and abiotic reactions in the biogeochemical Fe cycle. *Nat. Rev. Microbiol.* **2014**, doi:10.1038/nrmicro3347.
(191) Roden, E. E.; Sobolev, D.; Glazer, B.; Luther, G. W. Potential for microscale bacterial Fe redox cycling at the aerobic-anaerobic interface, *Geomicrobiol. J.* **2004**, *21*, 379–391.

709

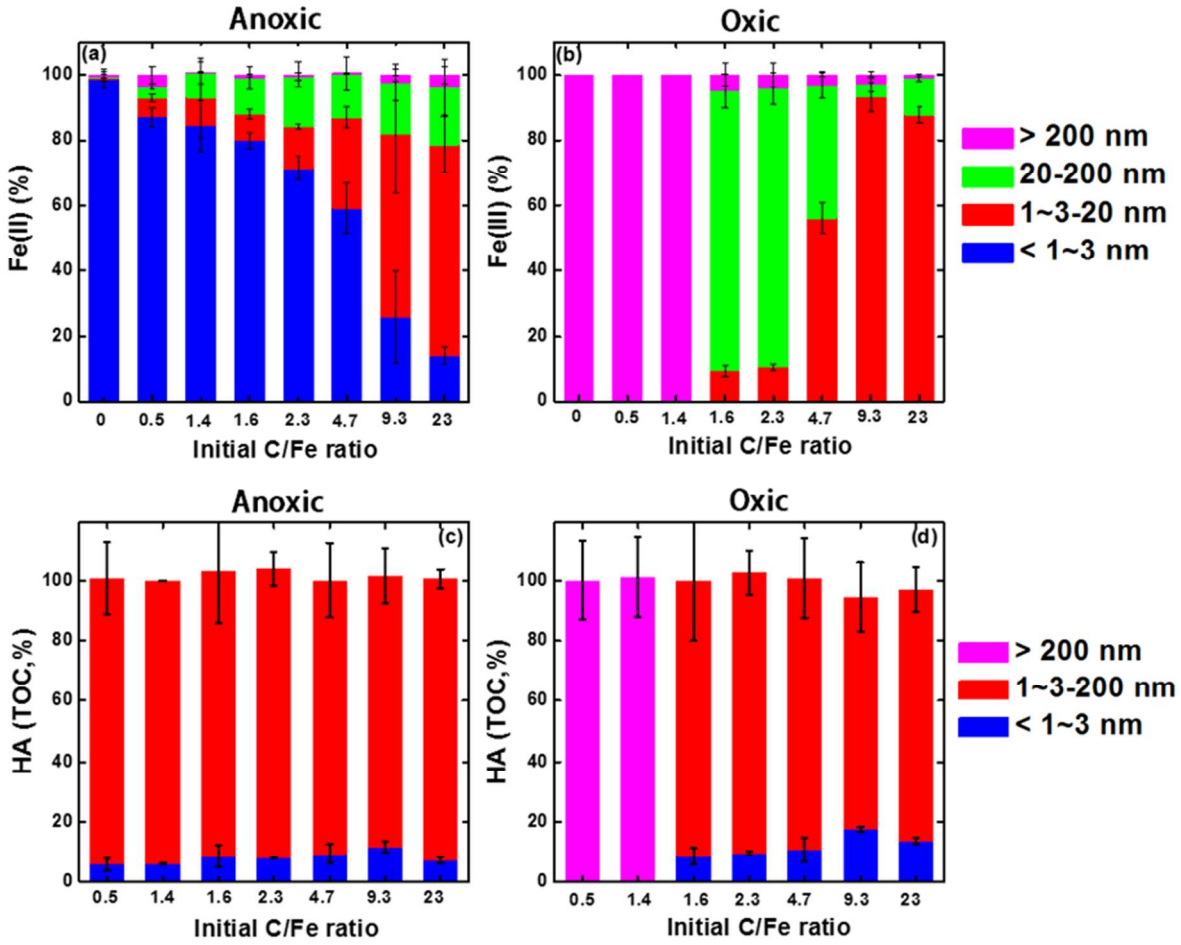

710
711

712 **Figure 1.** Percentage of (a,b) Fe and (c,d) HA concentrations in different size fractions at
713 (a,c) anoxic and (b,d) oxic steady-state conditions as a function of initial C/Fe molar
714 ratios. The percentage in y-axis means the concentration of Fe and HA in a certain size
715 fraction to the total concentration of Fe and HA in the suspension. Please note that all Fe
716 in the anoxic samples was Fe(II) and all Fe in the oxidized samples was Fe(III). Error
717 bars represent standard deviations of triplicate measurements.
718

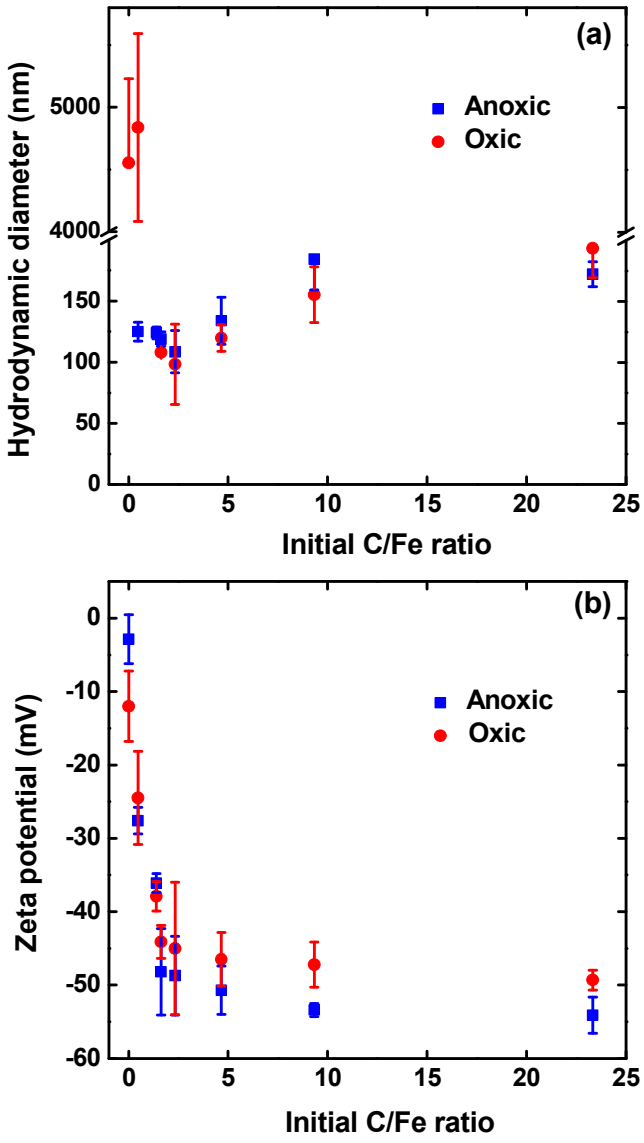

Figure 2. (a) Z-averaged hydrodynamic diameter and (b) zeta potential of colloids and larger particles in HA-Fe suspension at anoxic and oxic steady-state conditions as a function of initial C/Fe molar ratios. Error bars represent standard deviations of triplicate measurements.

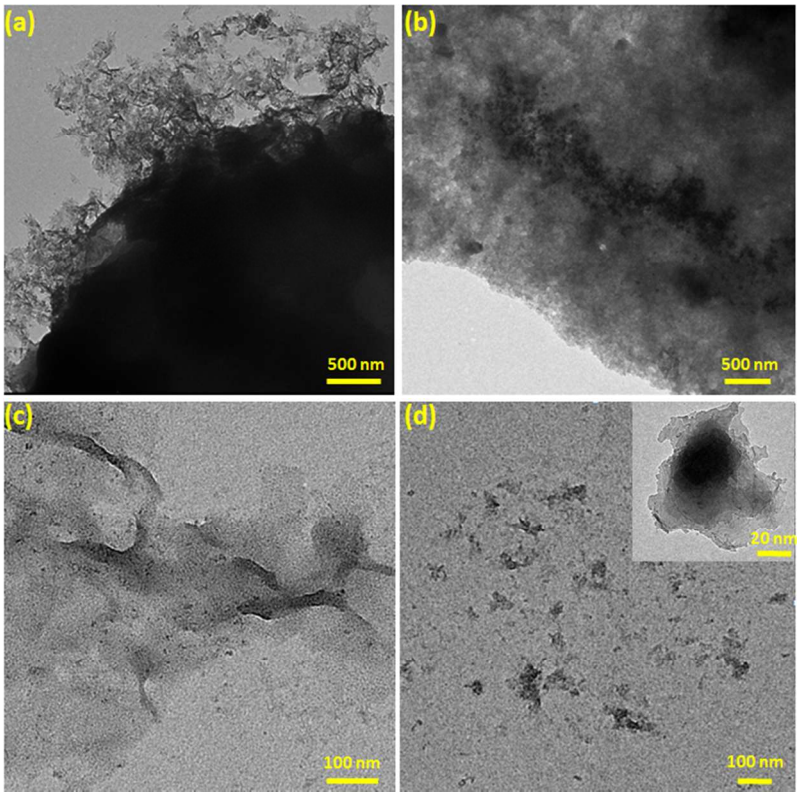

Figure 3. TEM observation of different initial C/Fe molar ratios suspension at oxic steady-state conditions. (a) C/Fe = 0.5; (b) C/Fe = 1.4; (c) C/Fe = 4.7; (d) C/Fe = 23.3. The insert in panel d represents the high magnification of micrograph.

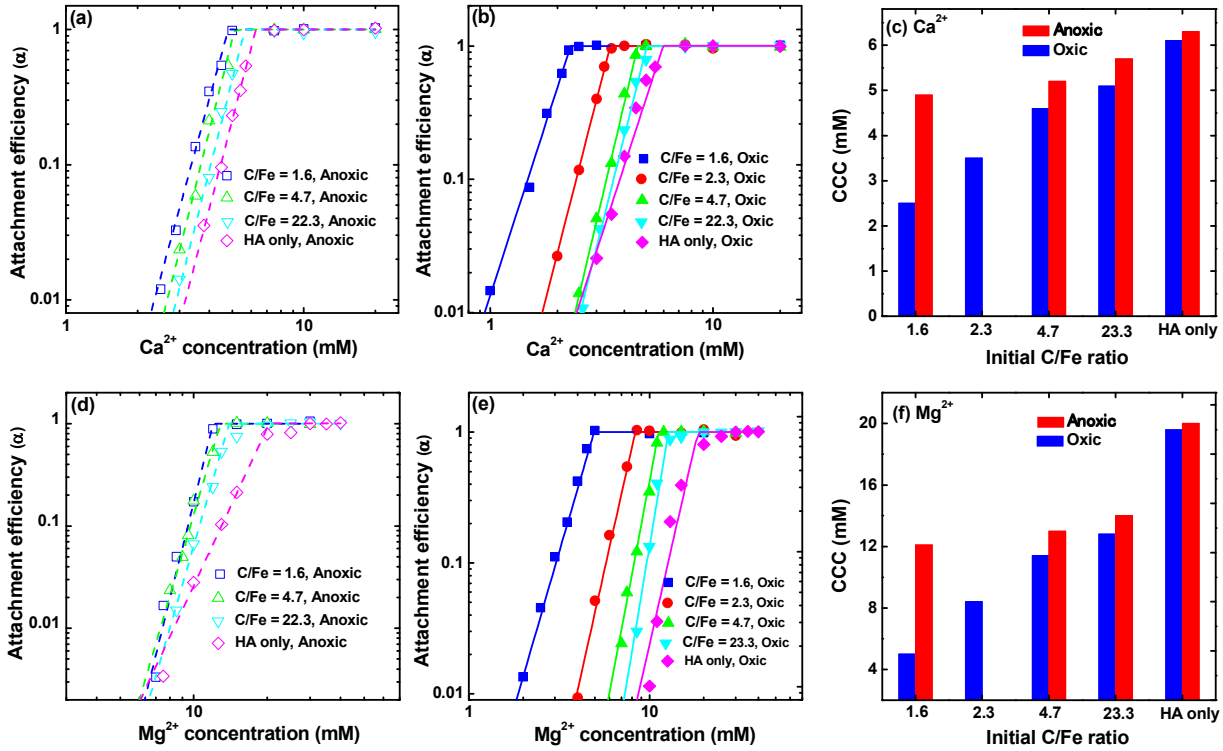

Figure 4. Attachment efficiency of HA-Fe colloids formed at (a, d) anoxic and (b, e) oxic conditions for different C/Fe molar ratios as a function of concentrations of (a, b) Ca^{2+} and (d, e) Mg^{2+} at pH 7. The corresponding critical coagulation concentration (CCC), which was summarized in panels c and f, was derived by intersection of extrapolations through reaction-limited and diffusion-limited regimes as an index of particle stability.

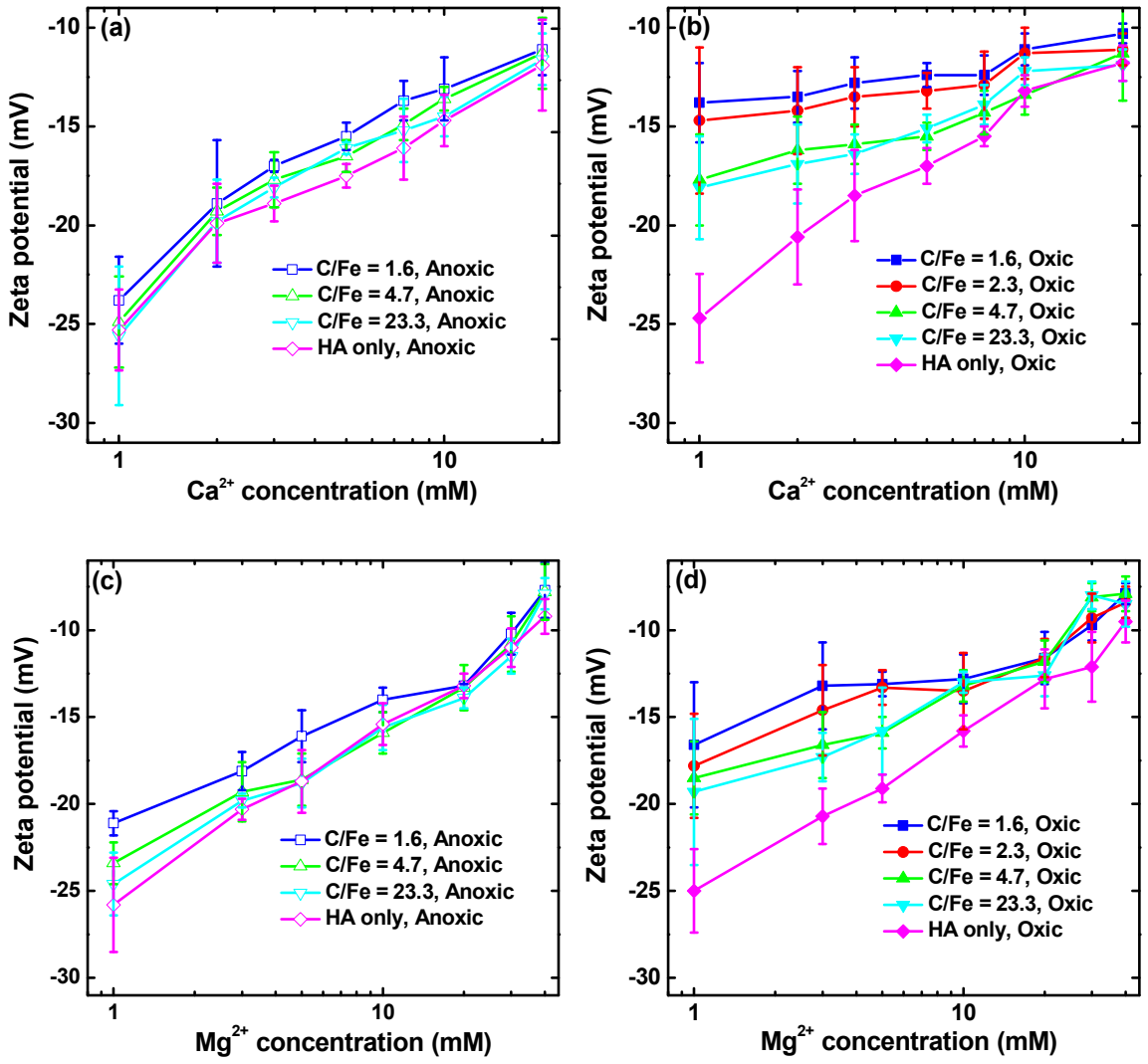

Figure 5. Zeta potentials of different C/Fe molar ratios of HA-Fe colloids formed at (a, c) anoxic and (b, d) oxic conditions respectively over a range of (a, b) Ca^{2+} and (c, d) Mg^{2+} concentrations at pH 7. Each data point shows the mean of 10 measurements of duplicate samples. Error bars represent standard deviations.

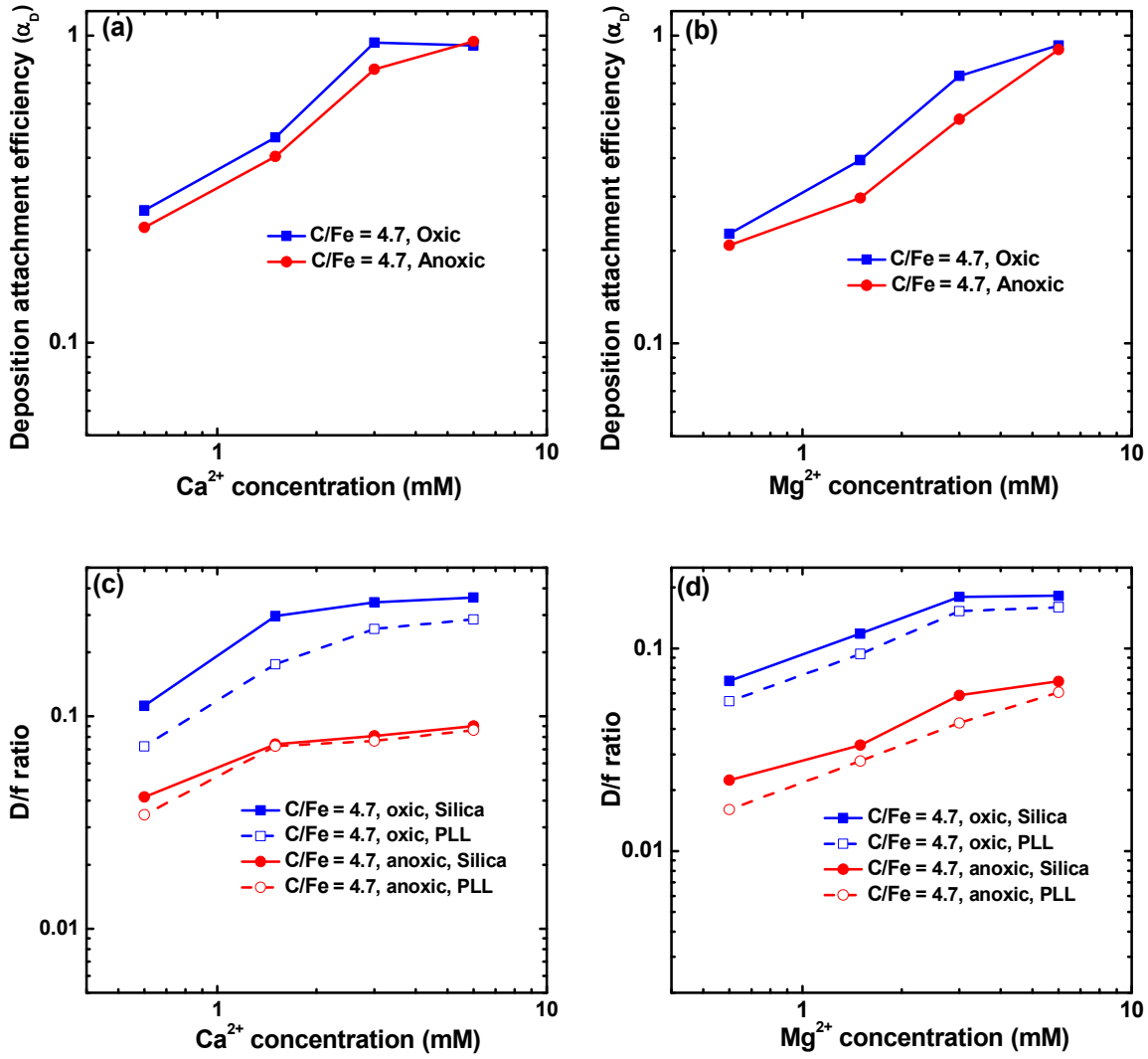

Figure 6. Deposition attachment efficiency of HA-Fe colloids formed at anoxic and oxic conditions in the presence of (a) Ca^{2+} and (b) Mg^{2+} onto silica surfaces. $|\Delta D(3)/\Delta f(3)|$ of HA-Fe colloids deposition in the presence of (c) Ca^{2+} and (d) Mg^{2+} onto silica and PLL surfaces.

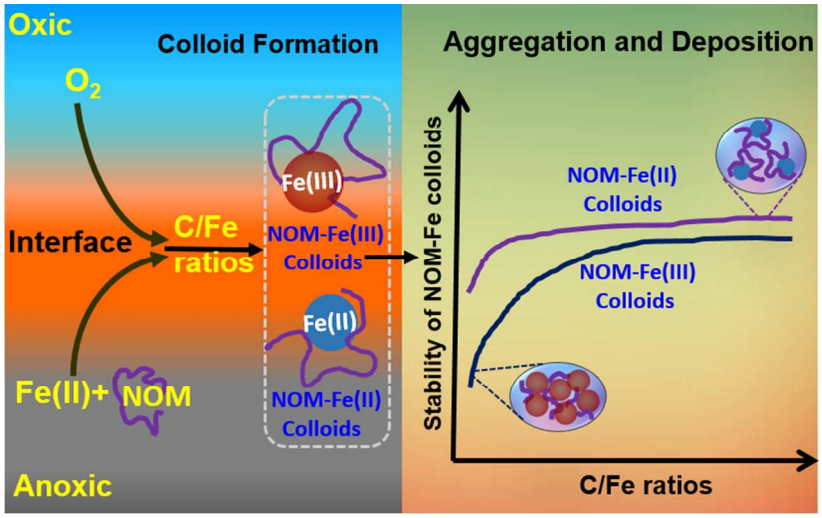
Oxic
Colloid Formation
Aggregation and Deposition
O2
Fe(III)
Interface
C/Fe ratios
NOM-Fe(III) Colloids
Fe(II)
Fe(II)+ NOM
NOM-Fe(II) Colloids
Anoxic
Stability of NOM-Fe colloids
NOM-Fe(II) Colloids
NOM-Fe(III) Colloids
C/Fe ratios

TOC